Stability of a self-similar adverse pressure gradient turbulent boundary layer

Eisfelder, M. P.; Müller, J. S.; Sekimoto, A.; Buchner, A. J.; Kitsios, V.; Atkinson, C.; Oberleithner, K.; Soria, J.

Publication date
2018

Document Version
Final published version

Published in
Proceedings of the 21st Australasian Fluid Mechanics Conference, AFMC 2018

21st Australasian Fluid Mechanics Conference
Adelaide, Australia
10-13 December 2018

Stability of a Self-Similar Adverse Pressure Gradient Turbulent Boundary Layer

M.P. Eisfelder[1], J.S. Müller[2], A. Sekimoto[1,3], A-J. Buchner[1,4], V. Kitsios[1,5], C. Atkinson[1], K. Oberleithner[2] and J. Soria[1]

[1]Laboratory for Turbulence Research in Aerospace and Combustion, Department of Mechanical and Aerospace Engineering, Monash University, Melbourne, VIC 3800, Australia
[2]Laboratory for Flow Instabilities and Dynamics, Technische Universität Berlin, Berlin 10623, Germany
[3]Department of Materials Engineering Science, Osaka University, Osaka 560-8531, Japan
[4]Laboratory for Aero and Hydrodynamics, Delft University of Technology, Delft 2628 CD, Netherlands
[5] CSIRO Oceans and Atmosphere, CSIRO, Battery Point, Tasmania 7004, Australia

Abstract

Linear stability analysis (LSA) of a self-similar adverse pressure gradient (APG) turbulent boundary layer (TBL) is explored in order to identify coherent structures. An eddy viscosity model (EV) is implemented via the Boussinesq hypothesis [8] to model the nonlinear coherent-turbulent interactions. Direct numerical simulations (DNS) by Kitsios et al. [3, 6] are used for the database of this study. A weak APG and strong APG (on the verge of separation) are studied with dimensionless streamwise pressure gradients (β) of 1 and 39 respectively. Their Reynolds numbers based on the momentum thickness (δ_2) within their respective regions of interest are $3,100-3,400$ and $10,000-12,300$. For the strong APG, the most unstable eigen-solution produces a wave resembling a Kelvin-Helmholtz (KH) instability located near the displacement thickness (δ_1) height. This position coincides with the inflection point (IP) in the mean flow profile. The IP satisfies Rayleigh's and Fjortoft's criterion for the existence of an inviscid instability [9]. Positive growth rate is seen for non-dimensional angular frequencies of $0.08 \leq \hat{\omega} \leq 0.51$, with the maximum growth occurring at $\hat{\omega} = 0.26$. The weak APG also contains a KH like wave, however for all $\hat{\omega}$, the growth rates are negative. Spanwise wavenumber $\hat{k_{x_r}}$ and phase velocity $\hat{c_r}$ increase monotonically for both β cases. Comparisons with a quasi-laminar analysis are also made.

Introduction

For many engineering flows, their performance is based directly on the flow's capacity to remain attached in the presence of an adverse pressure gradient (APG). These pressure gradients typically arise from complex convex curvatures. The ability to fully understand the effects of the pressure gradient is difficult due to the continuous change in the pressure gradient in the streamwise direction [5]. To overcome the upstream historical effects on the flow structure due to changes in pressure gradient, a canonical flow is required. Self-similarity allows the study of the dimensionless streamwise pressure gradient parameter:

$$\beta = \frac{\delta_1(\frac{\mathrm{d}P}{\mathrm{d}x})}{\tau_w} \tag{1}$$

with $\delta_1, \frac{\mathrm{d}P}{\mathrm{d}x}$ and τ_w respectively representing the displacement thickness, streamwise pressure gradient and wall shear stress. Whilst a constant β is desired, it is not a sufficient condition for there to be self-similarity. If the flow is self-similar, a self-similar function in terms of the non-dimensional wall-normal position η, where $\eta = y/\delta_1$ can be written for the velocity and Reynolds stresses. Full details of the requirements for a self-similar boundary layer are found in the works of George & Castillo [2], Castillo & George [1] and Kitsios et al. [3, 6]. Direct numerical simulations (DNS) by Kitsios et al. [3, 6] provide a database for a weak APG and strong self-similar APG with $\beta = 1$ and 39 respectively which are compared to investigate the influence of β on flow instabilities. The $\beta = 39$ represents a case where the flow is on the verge of separation. Their Reynolds numbers based on the momentum thickness (δ_2) within their regions of interest are $3,100-3,400$ and $10,000-12,300$. Velocities are scaled by the external velocity U_e.

Boundary layer characteristics and turbulent statistics

The mean profile of a flow provides information which is of great interest in linear stability analysis (LSA). The mean streamwise velocity profiles are shown in Figure 1 with the inflection points also marked. It is noted that the velocity profiles are similar for $y/\delta_1 < 0.02$ with the strong APG presenting lower velocities close to the wall compared to the weak APG up until δ_1. The second order statistics are presented in Figure 2 for $\beta = 1$ and $\beta = 39$ respectively. Comparisons to the modelled Reynolds stresses are discussed in the following section. Whilst the inner peak is still present, it is clear that the influence of the pressure gradient is to flatten this peak and to create a dominant outer peak at δ_1. As $\beta \to \infty$, $\tau_w \to 0$ and the outer peak increases in magnitude, becoming the dominant location in the boundary layer. This outer peak corresponds to the peak in turbulent production term in the kinetic energy budget equations. Due to the high β flow being reminiscent of a free shear layer at high β, an instability may exist at this location in the streamwise velocity profile. Simple criteria for the identification of an unstable flow exist in the form of Rayleigh's and Fjortoft's criteria. The Rayleigh inflection point theorem states that the flow is unstable if $U(y)$ has an inflection point (IP). However a more restrictive requirement comes from Fjortoft's criterion requiring that

$$\frac{\partial^2 U}{\partial y^2} \cdot (U - U_{IP}) < 0 \tag{2}$$

below and above the considered inflection point, with U_{IP} being the velocity at the inflection point [9]. For $\beta = 1$, the second derivatives reveal a single IP denoted as *I* and a saddle point at $\sim 1 < y/\delta_1 <\sim 2$. This IP satisfies both Rayleigh's and Fjortoft's criterion. The $\beta = 39$ case presents three IP. IP *I* satisfies both criteria with its location the same as in the $\beta = 1$ case, with *II* failing Fjortoft's criterion and *III* like *I* passing both criteria. The location of *I* however is too close to the wall, is dominated by viscous effects, and unable to sustain an instability. However *III* is located far enough from the wall to be removed from these effects and is a likely candidate for the existence of a Kelvin-Helmholtz (KH) instability.

Linear stability analysis methodolgy

The MAtrix Forming Instability Analysis (MAFIA) developed by Parades [7] is used to conduct the linear stability analysis (LSA). The LSA for turbulent flows is based on the Navier-Stokes equation of the coherent fluctuation velocity, linearised

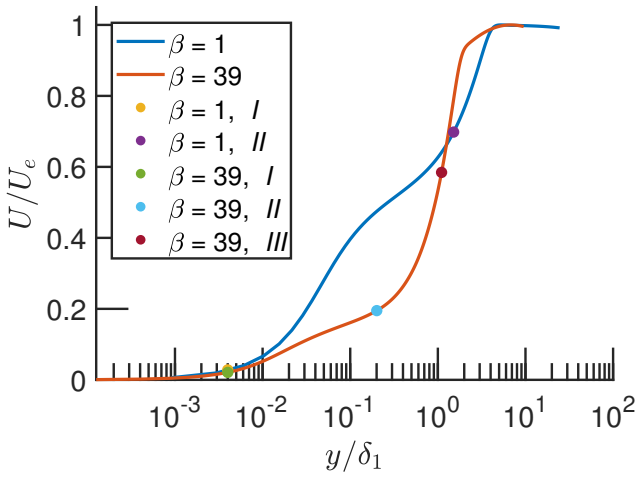

Figure 1: Wall-normal profile of the streamwise velocity profiles in the self-similar region of the DNS.

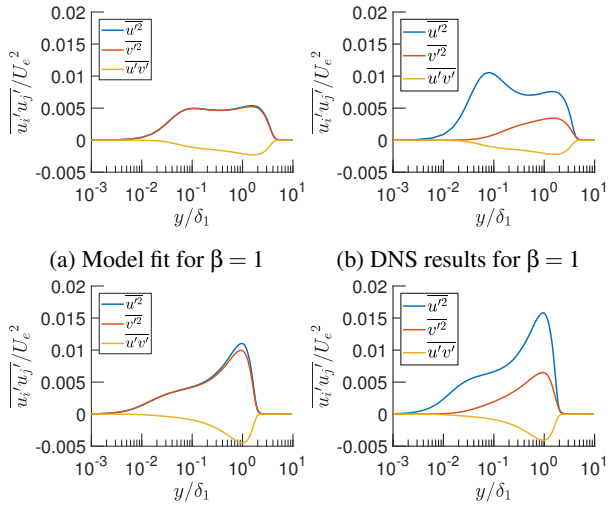

(a) Model fit for $\beta = 1$ (b) DNS results for $\beta = 1$

(c) Model fit for $\beta = 39$ (d) DNS results for $\beta = 39$

Figure 2: Reynolds stresses against wall-normal position.

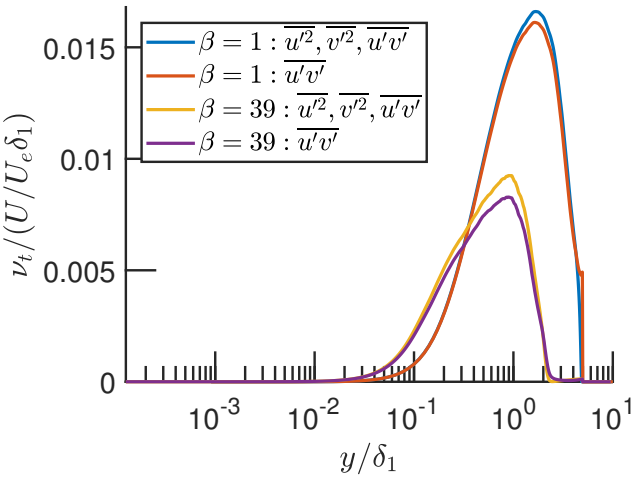

Figure 3: Modelled eddy viscosity ν_t as a function of wall-normal position.

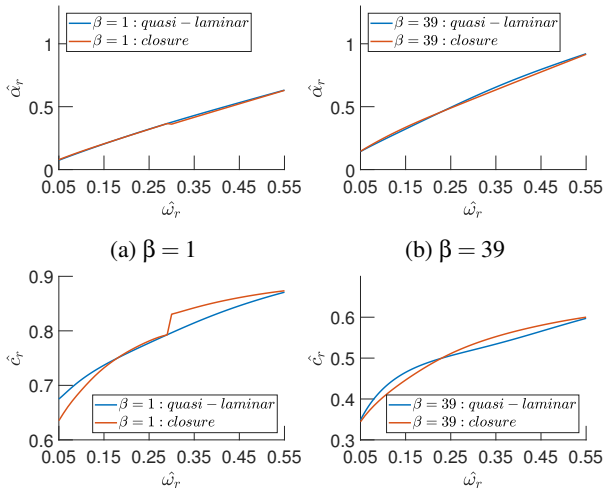

(a) $\beta = 1$ (b) $\beta = 39$

(c) $\beta = 1$ (d) $\beta = 39$

Figure 4: (a,b) Dispersion relationship of $\hat{\alpha}_r$ against $\hat{\omega}_r$. (c,d) Dispersion relationship of $\hat{c_r}$ against $\hat{\omega}_r$.

around the mean flow state. A normal mode ansatz

$$\mathbf{q}(x,y,z,t) = \hat{\mathbf{q}}(y) \cdot e^{i(k_x x + k_z z - \omega t)} \tag{3}$$

is substituted for the coherent part of the triple-decomposed velocity

$$\mathbf{q}(x,y,z,t) = \overline{\mathbf{q}}(x,y,z) + \tilde{\mathbf{q}}(x,y,z,t) + \mathbf{q}''(x,y,z,t). \tag{4}$$

In these equations $\overline{\mathbf{q}}$ represents the mean part of the velocity and pressure, with $\mathbf{q}'$ being the turbulent fluctuation, comprised of $\tilde{\mathbf{q}}$ and $\mathbf{q}''$ the coherent and turbulent-stochastic components respectively. To conduct the LSA, two of (k_x, k_z, ω) are specified, with these terms representing the streamwise wavenumber, spanwise wavenumber and temporal frequency respectively and their dimensionless counterparts given by $\hat{k_x}, \hat{k_z}, \hat{\omega}$. Solving the eigenvalue problem leads to the third variable as well as the amplitude (eigenfunction) $\hat{\mathbf{q}}$ of the solution. To solve this ansatz, a turbulence model is necessary for closure of the unknown Reynolds stresses. As shown in Reynolds and Hussain [8] and in Kitsios et al. [4, 5], the linearised Navier-Stokes equations for the coherent perturbation velocity contain additional terms resulting from the phase-averaged non-linear interactions between mean, coherent and stochastic field. However two simplifications can be made: the non-linear interaction between the coherent fluctuations is negligible ($\widetilde{\tilde{\mathbf{u}}\tilde{\mathbf{u}}} \approx 0$) and the coherent Reynolds stress is small compared to the stochastic part ($\widetilde{\tilde{\mathbf{u}}\tilde{\mathbf{u}}} \approx \mathbf{0}$). The remaining term which must be modelled is the coherent-stochastic interaction $\widetilde{\mathbf{u}''\mathbf{u}''}$. This can be modelled appropriately as

$$\widetilde{\mathbf{u}''\mathbf{u}''} = -2\overline{\nu_t}\tilde{\mathbf{S}} \tag{5}$$

where $\tilde{\mathbf{S}}$ is the coherent shear rate tensor and $\overline{\nu_t}$ is the eddy viscosity (EV). The argument can be made that no changes in eddy viscosity and turbulent kinetic energy contribution is made from the coherent perturbation, with these terms defined as $\tilde{\nu_t} = \mathbf{0}$ and $\tilde{k} = 0$ respectively. The modelling of $\overline{\nu_t}$ is found from a least square fit over all stochastic Reynolds stresses given by

$$\overline{\nu_t} = -\frac{\overline{\mathbf{u}''\mathbf{u}''}:\overline{\mathbf{S}}}{2\overline{\mathbf{S}}:\overline{\mathbf{S}}} \tag{6}$$

with $\overline{\mathbf{u}''\mathbf{u}''}$ representing the stochastic Reynolds stress tensor, $\overline{\mathbf{S}}$ the mean strain rate tensor and the operation : being the Frobenius product. The least square fit for $\overline{\nu_t}$ contains all nine components of $\overline{\mathbf{u}''\mathbf{u}''}$ and $\overline{\mathbf{S}}$. To simplify these terms, it can be assumed

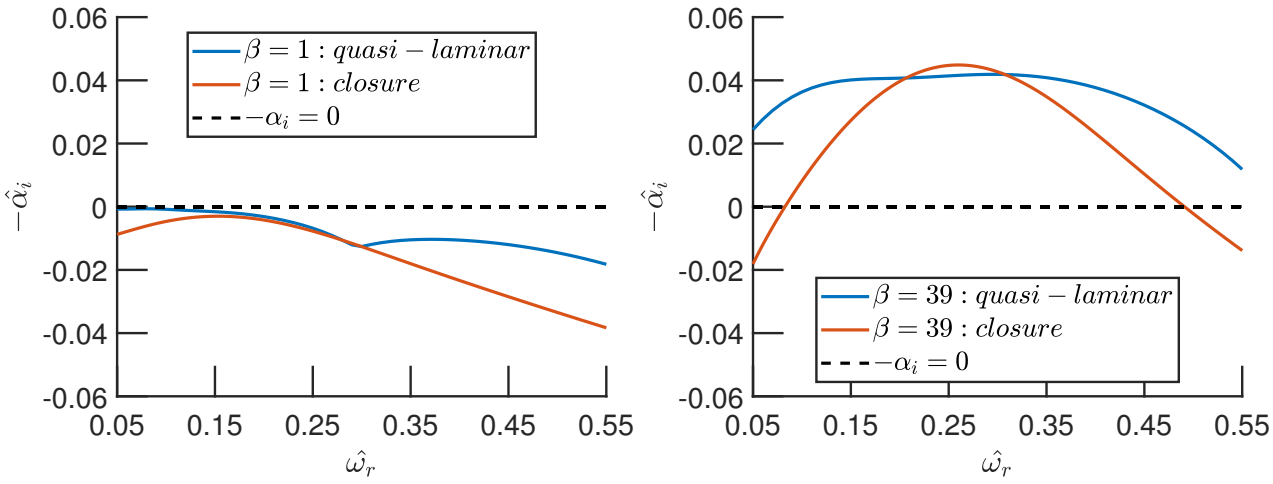

(a) $\beta = 1$ (b) $\beta = 39$

Figure 5: Dispersion relationship of $-\hat{\alpha}_i$ against $\hat{\omega}_r$. Neutral growth is indicated with the line $-\hat{\alpha}_i = 0$.

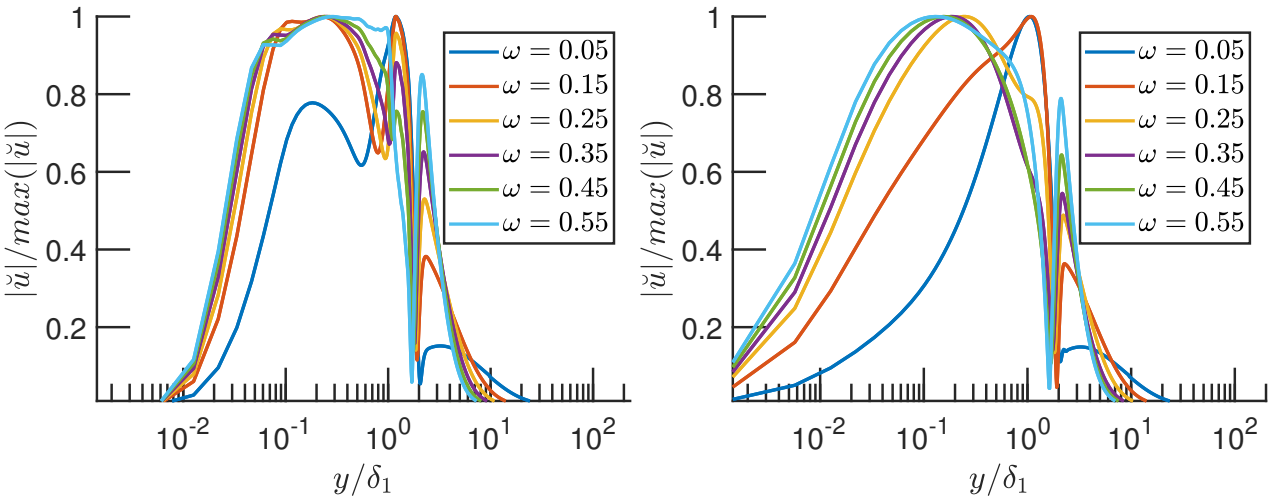

(a) $\beta = 39$ quasi-laminar (b) $\beta = 39$ with the closure model

Figure 6: Modulus of the streamwise eigenfunctions.

all spanwise gradients are zero i.e. $\frac{\partial \overline{u}}{\partial z} = \frac{\partial \overline{v}}{\partial z} = \frac{\partial \overline{w}}{\partial z} = 0$. Additionally, there is no mean spanwise velocity. Furthermore, the stochastic shear stresses in the x—z and y—z direction are zero due to homogeneity, i.e. $\overline{u''w''} = \overline{v''w''} = 0$. Since the stochastic Reynolds stresses $\mathbf{u''u''}$ are not known *a priori*, they will be approximated by the turbulent Reynolds stresses, i.e. $\mathbf{u''u''} \approx \mathbf{u'u'}$. It is found that without this closure, the quasi-laminar model does not produce the correct results.

The flexibility of MAFIA allows for a variety of both discretisation schemes and solving algorithms. The discretisation of the field is implemented with 400 Chebyshev collocated grid points (mesh independence above this many grid points) with piecewise polynomials of degree 16 as a finite difference scheme implementation. The solution is found via an Arnoldi iteration scheme. The mean profile is extended such that at the far field boundary conditions are $y/\delta_1 = 500$, $U/U_e \approx 1$. On the wall, homogeneous Dirichlet conditions are set for the coherent velocity fluctuations and a homogeneous Neumann condition for the coherent pressure fluctuation. In the far field homogeneous Dirichlet conditions are imposed for all fluctuations.

The influence of the turbulence model to account for the coherent-turbulent stresses will be now compared. The Reynolds stress term is dominated by $\overline{u'v'}$, with the results without the normal stresses found to not change significantly. The results of $\overline{\nu_t}$ as a function of wall normal distance are presented in Figure 3 and show that the peaks of additional viscosity are present around δ_1. The influence of $\overline{u'v'}$ being the dominant term is consistent with the findings of Kitsios et al. [4] for flows with spanwise homogeneous statistics. Reynolds stresses modelled with $\overline{\nu}_t$ and the mean kinetic energy $\overline{k}$, via the Boussinesq hypothesis [8] show that the highly anisotropic stresses in the simulation become more isotropic resulting in $\overline{u'^2}$ too low and $\overline{v'^2}$ too high as shown in Figure 2. Of interest is the peak stress located near the mean velocity inflection point. Figure 2a shows that for the weak APG, the stresses are also anisotropic but the shapes are not similar. There is a mismatch in shape and value of $\overline{u'^2}$ with the inner peak less dominant and similar in size to the outer peak.

Results and discussion

Performing a spatial stability analysis, with $\hat{k_{z_r}} = 0$, reveals little change in $\hat{k_{x_r}}$ against $\hat{\omega}_r$ with increasing monotonic growth

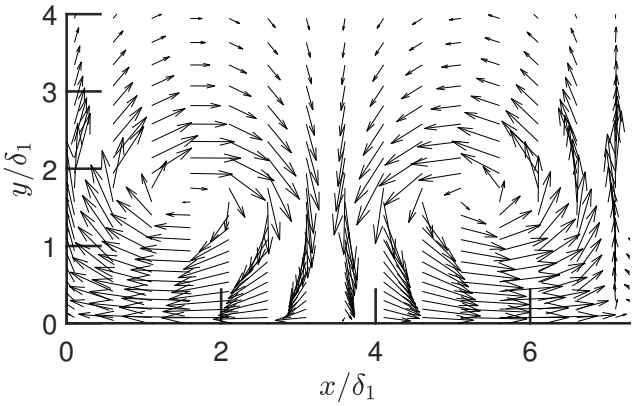

Figure 7: A sample of the vortices and roll-up phenomena generated in the KH instability for the most amplified mode ($\hat{\omega} = 0.51$, $\hat{k_{x_r}} = 0.86$) and $\beta = 39$. The KH instability is shown for one axial wavelength in streamwise direction. The arrows indicate the coherent fluctuation component only.

as evident in Figure 4a and 4b for both β cases with the effect of the additional viscosity being negligible. The changes in phase velocity ($\hat{c_r}$) are shown in Figure 4c and 4d with increasing monotonic growth also present and again minimal difference between having the closure model present or not. When the closure model is not present, $\hat{c_r}$ displays a decrease in slope at higher frequencies. Growth rates ($-\alpha_i$) are presented in Figure 5 with the neutral growth line also included. Unstable growth for the strong APG is found for $0.08 \leq \hat{\omega} \leq 0.51$ with a peak at $\hat{\omega} = 0.26$. For the weak APG all frequencies are stable in the dispersion relation. Therefore, a KH instability occurs only for the strong APG, while it is absent for the weak APG case. The streamwise growth rate, $-\alpha_i$, against frequency, reveals the response after the peak frequency to be double for the strong APG compared to the weak APG case. Without the closure model, the region for unstable growth increases for $\beta = 39$ and peak growth occurs at $\hat{\omega} = 0.33$. For $\beta = 1$ without the closure, a secondary peak is introduced, originating from $\hat{\omega} = 0.3$ and maxima at $\hat{\omega} = 0.4$. For $\hat{\omega} < 0.2$, the growth rates compared to the EV model case are reduced for $\beta = 1$, thus demonstrating the significance of the EV closure model.

The effect of increasing β is also evident in that it causes a transition from a stable KH wave to an unstable one at some stage. The magnitudes of the unstable streamwise eigenfunctions as a function of wall-normal coordinate and frequency can be seen in Figure 6. By examining the changes in these figures, it is evident that the role of the closure model removes a secondary peak around δ_1 for some intermediate $\hat{\omega}$.

An example of the KH wave can be seen in Figure 7 for the most amplified frequency of $\hat{\omega} = 0.51$ in the strong APG case of $\beta = 39$. Here, the streamwise and wall-normal eigenfunction, representing the coherent fluctuation, are shown as velocity vectors. The eigenfunctions are periodically continued in streamwise direction with the corresponding wavenumber of $\hat{k_{x_r}} = 0.86$. Examining Figure 7 it is clear that the KH wave displays the typical roll-up phenomena which takes several δ_1 to take effect in the streamwise direction. The location of the instability occurs at around δ_1, in line with the peak Reynolds stresses, inflection point satisfying Fjortoft's criterion and matching the maximum modulus of the streamwise eigenfunctions. The wall-normal eigenfunctions for all cases discussed (not shown) display a peak at $y/\delta_1 \approx 2$ before decaying farther away from the wall.

Conclusion

Linear stability analysis is performed on a weak and strong APG TBL with $\beta = 1$ and $\beta = 39$ provided by Kitsios et al. [3, 6]. Using the MAFIA solver of Paredes [7] and undertaking a spatial analysis, it is found that the flow is stable for all $\hat{\omega}$ for $\beta = 1$ whilst for $\beta = 39$ it is unstable for $0.08 \leq \hat{\omega} \leq 0.51$. The instability mode present takes the form of a KH wave and is only present for the strong APG case near δ_1.

Acknowledgements

The authors would like to acknowledge the research funding by the Australian Government through the Australian Research Council, The Australia-Germany Joint Research Cooperation Scheme an initiative of Universities Australia and the German Academic Exchange Service (DAAD) and the computational resources provided by the Australian National Computational Infrastructure and The Pawsey Supercomputing Centre through the National Computational Merit Allocation Scheme.

References

[1] Castillo, L. & George, W. K. (2001). Similarity Analysis for Turbulent Boundary Layer with Pressure Gradient: Outer Flow. *AIAA Journal*, **39**, **1**, 41-47.

[2] George, W. K. & Castillo, L. Boundary layers with pressure gradient: another look at the equilibrium boundary layer. *In Near Wall Turbulence*. Elsevier, 1993.

[3] Kitsios, V., Atkinson, C., Sillero, J., Borrell, G., Gungor, A., Jimenez, J., & Soria, J. (2016).Direct numerical simulation of a self-similar adverse pressure gradient turbulent boundary layer. *Intl J. Heat Fluid Flow*, **61**, 129-136.

[4] Kitsios, V., Cordier, L., Bonnet, J., Ooi, A., & Soria, J. (2010). Development of a nonlinear eddy-viscosity closure for the triple-decomposition stability analysis of a turbulent channel. *J. Fluid Mech*, **664**, 74-107.

[5] Kitsios, V., Cordier, L., Bonnet, J., Ooi, A., & Soria, J. (2011). On the coherent structures and stability properties of a leading-edge separated aerofoil with turbulent recirculation.c *J. Fluid Mech*, **683**, 395-416.

[6] Kitsios, V., Sekimoto, A., Atkinson, C., Sillero, J., Borrell, G., Gungor, A., Jimenez, J., & Soria, J. (2017). Direct numerical simulation of a self-similar adverse pressure gradient turbulent boundary layer at the verge of separation. *J. Fluid Mech*, **829**, 392-419.

[7] Paredes, P. (2014). *Advances in global instability computations: From incompressible to hypersonic flow*. PhD Thesis, Universidad Politecnica de Madrid.

[8] Reynolds, W., & Hussain, A. (1972). The mechanics of an organized wave in turbulent shear flow. Part 3. Theoretical models and comparisons with experiments. *Journal of Fluid Mechanics*, **54(2)**, 263-288.

[9] Schmid, P. J. & Henningson, D. S. , *Stability and Transition in Shear Flows*. Springer, 2001.